Kobe University Repository : Kernel

PDF issue: 2025-12-04

The Impact of the Next-Nearest Neighbor Dispersion Interactions on Spin Crossover Transition Enthalpy Evidenced by Experimental and Computational Analyses of Neutral pi-…

Miyawaki, Atsuhiro
Mochida, Tomoyuki
Sakurai, Takahiro
Ohta, Hitoshi
Takahashi, Kazuyuki

(Citation)
Inorganic Chemistry,59(17):12295-12303

(Issue Date)
2020-09-08

(Resource Type)
journal article

(Version)
Accepted Manuscript

(Rights)
This document is the Accepted Manuscript version of a Published Work that appeared in final form in Inorganic Chemistry, copyright © American Chemical Society after peer review and technical editing by the publisher. To access the final edited and published work see https://doi.org/10.1021/acs.inorgchem.0c01378

(URL)
https://hdl.handle.net/20.500.14094/90007491

The Impact of the Next-nearest Neighbor Dispersion Interactions on Spin Crossover Transition Enthalpy Evidenced by Experimental and Computational Analyses of Neutral π-extended Heteroleptic Fe(III) Complexes

Atsuhiro Miyawaki,[†] Tomoyuki Mochida,[†,‡] Takahiro Sakurai,[§] Hitoshi Ohta,[¶] and Kazuyuki Takahashi*,[†]

†Department of Chemistry, Graduate School of Science, Kobe University, 1-1 Rokkodai-cho, Nada-ku, Kobe, Hyogo 657-8501, Japan

‡Center for Membrane and Film Technology, Kobe University, 1-1 Rokkodai-cho, Nada-ku, Kobe, Hyogo 657-8501, Japan.

§Research Facility Centre for Science and Technology, Kobe University, 1-1 Rokkodai-cho, Nada-ku, Kobe, Hyogo 657-8501, Japan.

¶Molecular Photoscience Research Centre, Kobe University, 1-1 Rokkodai-cho, Nada-ku, Kobe, Hyogo 657-8501, Japan

ABSTRACT: A neutral heteroleptic Fe(III) complex **1** derived from π-extension of the parent complex **2** was prepared and characterized. Complex **1** exhibited an abrupt spin crossover (SCO) transition exactly at room temperature (T_{SCO} = 298 K). The crystal structure analysis of **1** revealed that the Fe(III) complex molecules formed a three-dimensional π-stacking interaction network. To clarify the mechanism of the SCO transition thermodynamically, the thermodynamic parameters of the SCO transitions for **1** and **2** were deduced from the temperature dependence of magnetic susceptibility in the solid- and solution-states by using the regular solution model. The comparison of the SCO enthalpy difference between the solid and molecule for **1** and **2** revealed that the lattice enthalpy difference would largely contribute to the SCO transition enthalpy difference. The computational evaluation of intermolecular interactions and lattice energies before and after the SCO transitions in **1** and **2** disclosed a significant contribution of the next-nearest neighbor dispersion interactions to the lattice enthalpy differences. This finding indicates that not only conventional nearest neighbor intermolecular interactions but also the next-nearest neighbor dispersion interactions should be taken into account to comprehend the fundamental mechanism of a phase transition in molecular solids.

INTRODUCTION

Switching phenomena of the electronic state and structure of a substance have aroused a wide-spread interest in chemical and materials science. In particular, switching of a property in an inorganic solid is recognized as a solid-state phase transition and can be used for practical applications to storage, memory, display, and sensing devices. On the other hand, the design and synthesis of a new molecular solid that exhibits a phase transition around room temperature is still a challenging issue.

Spin crossover (SCO) between high-spin (HS) and low-spin (LS) states is one of the switching phenomena in a transition metal coordination compound.[1–3] Since SCO accompanies a change in both the electronic state and coordination structure, SCO compounds have recently attracted much attention to potential switching materials for sensors and actuators.[4,5] Furthermore, multifunctional SCO hybrids such as SCO conductors,[6–8] SCO magnets[9–12], SCO ferroelectrics,[13] and SCO optics[14–16] have been developed.

Solid-state SCO transitions around room temperature were sometimes reported in the literature,[17,18] but their fundamental mechanisms at the molecular level have scarcely been understood. From a thermodynamic point of view, the transition temperature ($T_{1/2}$) in a solid-state phase transition including SCO is determined by

$$T_{1/2} = \frac{\Delta H}{\Delta S} \cdots (1)$$

where ΔH is the enthalpy difference and ΔS is the entropy difference between two phases. For SCO solids, it is widely accepted that ΔS is derived mainly from the differences in spin multiplicity and intramolecular vibration between the HS and LS states,[19,20] and drives SCO. On the other hand, ΔH is conceived to originate mainly from the energy difference between the HS and LS molecules,[21] but other quantitative contributions have not been stated clearly. The differences in SCO behavior between polymorphs and solvates suggest the significant contribution of crystal-packing effect to ΔH in SCO transition. Very recently the possibility of the important contribution of intermolecular interactions to ΔH in SCO transition was proposed.[22,23] Therefore, we focused on the clarification of the impact of intermolecular interactions on the enthalpy differences ΔH concerning SCO transition.

To evaluate the contribution of intermolecular interactions to the thermodynamic parameters in SCO, we can decompose the SCO transition enthalpy $\Delta_{cry}H$ and entropy $\Delta_{cry}S$ in the solid-state into the molecular terms, $\Delta_{mol}H$ and $\Delta_{mol}S$, and the

crystal-lattice terms, $\Delta_{lat}H$ and $\Delta_{lat}S$. In these parameters, $\Delta_{cry}H$ and $\Delta_{cry}S$ can be determined experimentally by differential scanning calorimetry (DSC) and the temperature dependence of magnetic susceptibility for a crystalline sample, and $\Delta_{mol}H$ and $\Delta_{mol}S$ can also be estimated by the temperature dependence of magnetic susceptibility for a solution sample. On the other hand, it is very difficult to evaluate $\Delta_{lat}H$ and $\Delta_{lat}S$ for an SCO compound experimentally. Although $\Delta_{lat}H$ is closely related to intermolecular interactions, the calculation of intermolecular interactions for metal coordination compounds by the accurate quantum mechanical model is usually time-consuming and difficult. CrystalExplorer 17 (CE17)[24] developed by Spackman et al. can calculate the interaction energy of the CE-B3LYP energy model that is based on the sum of scaled four energy components.[25,26] Among four energy components, electrostatic, polarization, and exchange-repulsion energies are calculated using unperturbed monomer wavefunctions at the B3LYP/6-31G(d,p) level, and dispersion energy is estimated from Grimme's dispersion correction. The scale factors of the four energy components were determined by fitting to B3LYP-D2/6-31G(d,p) counterpoise-corrected energies of various kinds of organic, inorganic, metal-organic molecular compounds. The CE-B3LYP energy model reproduces B3LYP-D2/6-31G(d,p) counterpoise-corrected energies with a mean absolute deviation of 2.4 kJ mol^{-1}.[26] Although the CE-B3LYP energies exhibit systematic overestimates against benchmark CCSD(T)/CBS energies, the mean absolute deviation is 2.5 kJ mol^{-1}.[25] Thus the CE-B3LYP energy model can calculate intermolecular interaction and lattice energies[27] quantitatively and disclose the contribution of four energy components to the intermolecular interaction qualitatively at much inexpensive calculation cost.Thus, we utilized CE17 to estimate the intermolecular interactions and lattice energies $\Delta_{lat}H$ in SCO compounds and will discuss the impact of intermolecular interactions on the enthalpy difference in the solid-state SCO transitions.

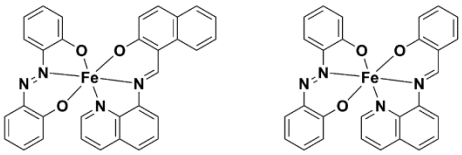

Figure 1. Molecular-structure formulas for [Fe(azp)(qnal)] (**1**) and [Fe(azp)(qsal)] (**2**).

To exclude the influence of large long-range Coulomb interactions between positive and negative charges, we selected neutral heteroleptic Fe^{III} SCO compounds, a new π-extended compound, [Fe(azp)(qnal)] (**1**) and its parent compound, [Fe(azp)(qsal)]·0.5CH_3OH (**2**)[28] (Figure 1) [Hqnal = *N*-(8-quinoyl)-2-hydroxy-1-naphthaldimine, H_2azp = 2,2'-azobisphenol, Hqsal = *N*-(8-quinoyl)salicylaldimine]. Since the crystal structures of **1** and **2** were constructed purely by π-stacking interactions, we can investigate the pure effects of π-stacking interactions on the SCO transition behaviors. Note that the π-extended derivative **1** exhibited an SCO transition exactly at room temperature. The comparison of the experimental thermodynamic parameters and computed intermolecular interaction energies revealed that the change in the next-nearest neighbor dispersion interactions as well as the nearest neighbor π-stacking interactions may play a crucial role in the enthalpy difference in SCO transition, leading to increasing the transition temperature to room temperature.

RESULTS

Synthesis of 1. A new π-extended complex **1** was synthesized by the ligand exchange reaction between the corresponding homoleptic [Fe(qnal)$_2$][7] and [Fe(azp)$_2$][29] complexes in acetonitrile solutions according to the literature.[28] The composition of obtained black platelet crystals was confirmed by microanalysis and single-crystal X-ray structure analysis.

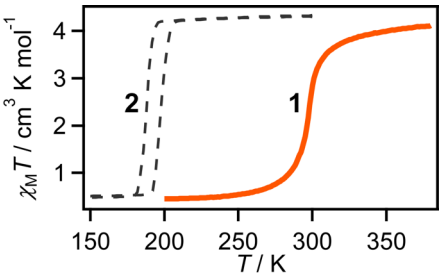

Figure 2. The $\chi_M T$ vs. T products for **1** (orange curve) and **2** (black broken curves)[28] in the solid-state.

Magnetic Susceptibility of 1 in the solid-state. The temperature variations of magnetic susceptibility for **1** were measured by a Quantum Design MPMS-XL magnetometer at 0.5 T in the temperature range of 200−380 K (Figure 2). The $\chi_M T$ value for **1** was 4.11 cm^3 K mol^{-1} at 380 K, suggesting that **1** was in the HS state, whose spin-only value is 4.38 cm^3 K mol^{-1}. On lowering temperatures, the $\chi_M T$ values for **1** were almost constant down to 310 K and then decreased steeply. Note that a magnetic transition was centered exactly at room temperature ($T_{1/2}\downarrow$ = 298 K). Further cooling the $\chi_M T$ value reached to 0.50 cm^3 K mol^{-1} at 200 K, indicating that the complex was in the LS state, whose spin-only value is 0.38 cm^3 K mol^{-1}. On heating the sample, a reverse transition occurred at the same temperature ($T_{1/2}\uparrow$ = 298 K), revealing that the magnetic transition accompanied no thermal hysteresis. As described in the crystal structure analysis below, this magnetic transition originated from the SCO transition. The transition temperature in the π-extended compound **1** was 110 K higher than that in the parent compound **2**,[28] whereas a thermal hysteresis disappeared in **1**.

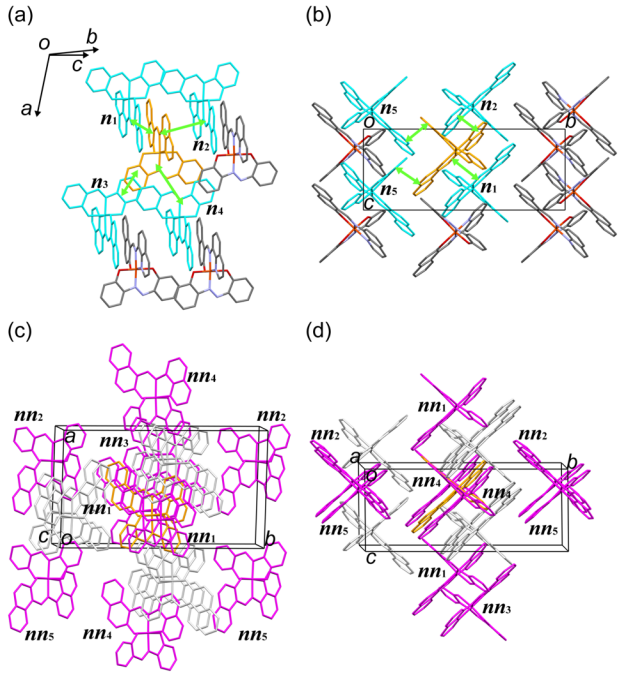

Figure 3. Packing diagrams of **1** at 90 K. (a) Top view of a two-dimensional π-stacking interaction layer. (b) Side view of the overlaps between the 2D layers. (c) View along the *c* axis. (d) View along the *a* axis. The nearest neighbor and next-nearest neighbor molecules of a yellow-colored molecule are indicated by cyan molecules with symbols of n_1–n_5 and magenta ones with symbols of nn_1–nn_5, respectively. Green double-headed arrows are depicted for clarity of the nearest neighbor interactions.

Crystal Structure for 1 at 90 and 373 K. To confirm the spin-state and structural changes upon the magnetic transition, the temperature variations of single-crystal X-ray analysis for **1** were performed by using a Bruker APEX2 ULTRA system. Fortunately, it was successful to determine the crystal structures for **1** at 90 and 373 K. The crystallographic data are listed in Table S1. The crystal belongs to the monoclinic system with $P2_1/c$ at both temperatures. The asymmetric unit contained one [Fe(azp)(qnal)] molecule. No orientational disorder was observed for the azp ligand although the homoleptic azp complexes often showed orientational disorder.[29] The divalent azp anion or monovalent qnal anion were coordinated to a Fe^{III} ion as tridentate ligands in an almost perpendicular manner, to construct a pseudo-octahedral FeN_3O_3 coordination sphere (Figure S1). The coordination bond lengths and distortion parameters (Σ, Θ, θ)[30] along with those of the parent compound **2** are listed in Table S2. The Fe-O and Fe-N coordination bond lengths in **1** at 373 K were in good agreement with those in the HS state of **2**, whereas those at 90 K were similar to those in the LS state of **2**. Moreover, the distortion parameters of Σ, Θ, and θ in **1** at 90 and 373 K were those in the low- and high-spin states of **2**, respectively. These indicate that compound **1** exhibited an almost complete SCO transition.

The molecular arrangement of the [Fe(azp)(qnal)] molecules in **1** at 90 K is depicted in Figure 3. The direct contacts of a Fe complex molecule with the nearest neighbor Fe complex molecules are designated as n_1–n_5, whose symmetry relationships are listed in Table S3. The top- and side-views for the π-overlaps n_1–n_4 are shown in Figure S2. The qnal ligands in **1** were stacked in two different manners. One π-overlap (n_1) between the whole qnal ligands in a head-to-tail manner was a π-plane distance of 3.33 Å, the other one between the quinolyl moieties (n_2) was that of 3.36 Å, forming a π-stacked one-dimensional (1D) molecular arrays along the *c* axis (Figure 3b). This π-stacking arrangement through the qnal ligands in **1** was very similar to that through the qsal ligands in **2**. Meanwhile, π-overlaps between the azp ligands in **1** were different from those in **2**. Although only the π-overlaps between the phenyl rings of the azp ligand were observed in **2**, one π-overlap between the whole azp ligands in a head-to-tail manner (n_4) was found to be a longer π-plane distance of 3.73 Å in **1**. The π-overlaps between the phenyl rings (n_3) similar to **2** was observed only at the side of the five-membered chelate ring in **1** (Figure 3a). The difference in the π-overlapping mode gave different two-dimensional (2D) layer structures between **1** and **2**. Note that a short C···C distance of 3.47 Å between the qnal ligands (n_5) was observed between the above mentioned 2D layers in **1** (Figure 3b).

The thermal variations of intermolecular π-plane and atom-atom distances are listed in Table 1. There was no significant change in the molecular arrangement of **1** at 373 K (Figure S2). Although the intermolecular distances at 373 K were a little longer than those at 90 K (Table 1), the intermolecular interactions were still effective as described in the computational analysis section.

Table 1. Intermolecular π-plane and atom-atom distances (Å) with the nearest neighbor Fe complex molecules (n_1–n_5) in **1**

Temp. / K	n_1	n_2	n_3	n_4	n_5[a]
90	3.33	3.36	3.32	3.73	3.47
373	3.39	3.37	3.43	3.84	3.53

[a] Interatomic distances

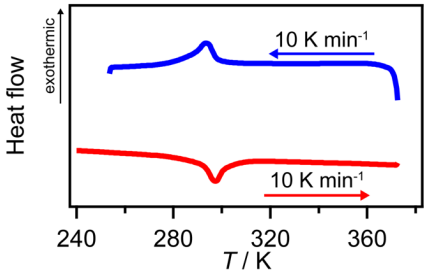

Figure 4. The DSC curves for **1**. The red and blue curves indicate the heating and cooling scans, respectively.

Thermal Analysis of 1 in the solid-state. To obtain the thermodynamic parameters for the solid-state SCO transition of **1**, the differential scanning calorimetry (DSC) for **1** was performed using a TA instruments Q100 differential scanning calorimeter. The DSC curves as a function of temperature are shown in Figure 4. On cooling the sample, a single exothermic peak was observed at 298.6 K with the enthalpy difference ΔH of 9.93 kJ mol^{-1} and entropy difference ΔS of 33.9 J K^{-1} mol^{-1}. On heating, a single endothermic peak also appeared at 289.9 K with ΔH = 9.16 kJ mol^{-1} and ΔS = 30.9 J K^{-1} mol^{-1}.

Magnetic susceptibility of 1 and 2 in the solution-state. To clarify the SCO behaviors of **1** and **2** at the molecular level, the temperature dependence of magnetic susceptibility of the chloroform solutions of **1** and **2** was determined by the Evans method[31] using a Bruker Avance 400 spectrometer. The $\chi_M T$ vs. T products for **1** and **2** are depicted in Figure 5. The $\chi_M T$

value in **1** was 3.1 cm^3 K mol^{-1}, and that in **2** was 3.8 cm^3 K mol^{-1} at 293 K. Both **1** and **2** exhibited a gradual decrease in the $\chi_M T$ value upon cooling, suggesting a gradual SCO conversion took place in **1** and **2**. The thermal dependence of the $\chi_M T$ in **2** is a little steeper than that in **1**.

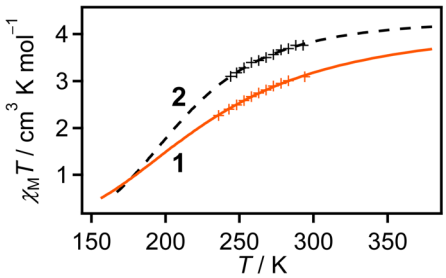

Figure 5. The $\chi_M T$ vs. T products for **1** (orange crosses) and **2** (black crosses) in the solution-state. The orange and black broken curves simulated from the best-fit parameters for **1** and **2**, respectively.

Thermodynamic Parameter Analysis for 1 and 2. To obtain the thermodynamic parameters of SCO in the solid-state and solution-state, the temperature variations of $\chi_M T$ in **1** and **2** in the solid-state and solution-state were fitted by the regular-solution model[32] expressed by

$$\ln\left[\frac{1-\gamma_{HS}}{\gamma_{HS}}\right] = \frac{\Delta H + \Gamma(1-2\gamma_{HS})}{RT} - \frac{\Delta S}{R} \cdots (2)$$

where γ_{HS} denotes the HS fraction, Γ denotes the interaction energy involving the cooperativity of SCO, and R is the gas constant. The subscripts "cry" and "solu" of thermodynamic parameters indicate the parameters in the solid-state and solution-state, respectively. The transition enthalpy and entropy in the solid-state were obtained by fitting the $\chi_M T$ vs. T plots in the enthalpy and entropy difference range between the cooling and heating DSC measurements. The interaction energy Γ_{solu} in the solution-state fixed zero. The best-fit parameters of **1** in the solid-state were $\Delta_{cry}H$ = 9.29 kJ mol^{-1}, $\Delta_{cry}S$ = 31.2 J K^{-1} mol^{-1}, and Γ_{cry} = 5.02 kJ mol^{-1} (Figure S3). The reported parameters of **2** in the solid-state were $\Delta_{cry}H$ = 5.33 kJ mol^{-1}, $\Delta_{cry}S$ = 28.7 J K^{-1} mol^{-1}, and Γ_{cry} = 3.50 kJ mol^{-1}.[28] These parameters reveal that the π-extension of the ligand leads to significant enhancement of $\Delta_{cry}H$ and Γ_{cry}, whereas it hardly affects $\Delta_{cry}S$. On the other hand, the thermodynamic parameters in the solution-state were $\Delta_{solu}H$ = 8.20 kJ mol^{-1} and $\Delta_{solu}S$ = 35.5 J K^{-1} mol^{-1} for **1**, and $\Delta_{solu}H$ = 11.8 kJ mol^{-1} and $\Delta_{solu}S$ = 55.6 J K^{-1} mol^{-1} for **2**, whose simulated curves are depicted in Figure 5. Although the thermodynamic parameters in the solid-state are in good agreement with those in the solution-state in **1**, that was not the case for **2**. This disagreement is discussed in the following discussion section.

Table 2. The nearest neighbor and the selected next-nearest neighbor intermolecular interaction energies (kJ mol^{-1})

	Symbol	N[a]	Sym. Op.[b]	Temp. / K	R[c] / Å	E_{ele}[d]	E_{pol}[e]	E_{dis}[f]	E_{rep}[g]	E_{tot}[h]	E_{lat}[i]	$\Delta_{lat}E$[j]
1	n_1	1	1−x, 1−y, 1−z	90	6.16	−97.0	−24.2	−179.0	194.3	−156.2	−78.1	2.9
				373	6.34	−75.6	−19.7	−167.0	144.9	−150.4	−75.2	
	n_2	1	1−x, 1−y, −z	90	8.52	−29.1	−8.1	−88.4	71.2	−69.8	−34.9	−1.55
				373	8.41	−26.8	−8.0	−89.6	63.9	−72.9	−36.45	
	n_3	1	−x, 1−y, 1−z	90	8.74	−25.6	−8.7	−87.3	71.7	−65.2	−32.6	4.4
				373	9.1	−13.4	−6.9	−73.9	44.2	−56.4	−28.2	
	n_4	1	−x, 1−y, −z	90	9.61	−6.3	−5.9	−55.0	36.9	−36.1	−18.05	1.6
				373	9.67	−0.8	−5.2	−52.1	27.9	−32.9	−16.45	
	n_5	2	x, 1/2−y, ±1/2+z	90	9.32	−12.8	−2.9	−51.4	40.9	−35.0	−35.0	1.5
				373	9.44	−9.9	−2.2	−45.4	29.5	−33.5	−33.5	
	nn_1	2	x, y, ±1+z	90	8.89	−1.5	−2.0	−25.5	13.2	−17.1	−17.1	4
				373	8.79	0.7	−1.6	−18.3	5.3	−13.1	−13.1	
	nn_2	2	1−x, ±1/2+y, 1/2−z	90	12.04	−4.3	−1.4	−12.3	6.1	−12.5	−12.5	1.3
				373	12.27	−3.3	−1.3	−12.2	6.2	−11.2	−11.2	
	nn_3	1	1−x, 1−y, 2−z	90	12.7	0.3	−0.1	−1.6	0	−1.2	−0.6	−0.1
				373	12.81	0	−0.1	−1.4	0	−1.4	−0.7	
	nn_4	2	±1+x, y, z	90	12.88	−0.9	−0.4	−5.3	1.1	−5.2	−5.2	−0.7
				373	13.14	−1.3	−0.5	−6.0	1.7	−5.9	−5.9	
	nn_5	2	−x, ±1/2+y, 1/2−z	90	13.19	−0.4	−0.2	−4.7	0.9	−4.2	−4.2	−0.1
				373	13.54	−0.4	−0.2	−5.4	1.5	−4.3	−4.3	
2	n_1	1	1−x, 1−y, 1−z	90	6.78	−47.6	−14.0	−106.8	77.9	−105.6	−52.8	−4.45
				273	6.44	−52.9	−16.3	−120.1	94.1	−114.5	−57.25	
	n_2	2	±1+x, y, z	90	8.21	−3.0	−5.6	−62.9	47.7	−32.6	−32.6	3.9
				273	8.35	0.1	−4.6	−52.1	32.3	−28.7	−28.7	
	n_3	1	1−x, −y, 1−z	90	8.27	−41.2	−10.5	−85.9	69.9	−82.9	−41.45	0.9
				273	8.3	−35.2	−9.9	−76.8	49.1	−81.1	−40.55	
	n_4	1	2−x, 1−y, 1−z	90	8.76	−23.6	−9.4	−61.7	38.4	−61.9	−30.95	−1.05
				273	9.07	−25.3	−8.6	−63.7	39.8	−64.0	−32.0	
	n_5	1	1−x, 1−y, 2−z	90	9.11	−11.7	−6.2	−60.9	55.1	−36.0	−18.0	−4.65
				273	9.05	−17.1	−5.1	−65.5	54.2	−45.3	−22.65	
	nn_1	1	2−x, 1−y, 2−z	90	8.75	3.8	−1.8	−25.4	9.3	−13.7	−6.85	3.4
				273	9.2	4.9	−1.3	−17.3	6.4	−6.9	−3.45	
	nn_2	1	2−x, −y, 1−z	90	11.23	−1.1	−0.2	−3.1	0	−4.0	−2.0	−0.05
				273	11.28	−1.2	−0.2	−3.0	0	−4.1	−2.05	
	nn_3	1	1−x, −y, 2−z	90	11.54	−1.2	−0.2	−3.5	0	−4.4	−2.2	0.7
				273	11.84	−1.3	−0.1	−1.8	0	−3.0	−1.5	
	nn_4	2	x, ±1+y, z	90	11.78	0.5	−0.3	−4.2	0.2	−3.2	−3.2	−0.2
				273	11.5	1	−0.4	−5.1	0.5	−3.4	−3.4	
	nn_5	2	x, y, ±1+z	90	11.95	−3.1	−0.8	−12.5	8	−9.9	−9.9	3.7
				273	12.59	−1.0	−0.6	−7.7	3.4	−6.2	−6.2	

[a] The number of molecules of the same environment. [b] Symmetry operation. [c] The separation of molecular centroid. [d] Electrostatic energy. [e] Polarization energy. [f] Dispersion energy. [g] Exchange-repulsion energy. [h] Total interaction energy. [i] Interaction energy contributed to lattice enthalpy. [j] Interaction energy difference contributed to lattice enthalpy difference.

Computational Analysis of Intermolecular Interactions for 1 and 2. The intermolecular interaction energies between two molecules in the LS and HS states for **1** and **2** were calculated at the CE-B3LYP model by CrystalExplorer17.[24] The electrostatic (E_{ele}), polarization (E_{pol}), dispersion (E_{dis}), exchange-repulsion (E_{rep}) energies are obtained from the corresponding calculation techniques,[26] and then the total energy (E_{tot}) is the sum of all the energies calibrated by the corresponding scale factors.[26] The interaction energies between the Fe complex molecules for **1** and **2** are listed in Table 2. The symbols of Table 2 for **1** and **2** indicate the positions shown in Figures 3 and S4, respectively. The nearest neighbor interac-

tions n_1–n_5 are the intermolecular interactions with the nearest neighbor Fe complex molecules having direct short contact with a central Fe complex molecule as described in the crystal structure description, whereas the next-nearest neighbor interactions nn_1-nn_5 are defined as the intermolecular interactions with five Fe complex molecules of the shortest distances between the molecular centroids except the nearest neighbor Fe complex molecules at 90 K. Although the interaction energies between the Fe complex and methanol molecules and between the methanol molecules in **2** were also calculated, the interaction energies between the methanol molecules are very small and hence can be ignored. All intermolecular interaction energies used for the calculation of lattice energies are also listed in Tables S5-S7.

The strongest intermolecular interaction energies E_{tot} between the Fe complex molecules were found in the π-overlaps (n_1) between the qnal molecules and between the qsal molecules in **1** and **2**, respectively. The interaction energy between the qnal molecules in **1** was about one and a half times as large as that between the qsal molecules in **2** in the LS and HS states. This indicates that the π-extension with one phenyl ring significantly enhanced the intermolecular interaction energy. The other interaction energies between the nearest neighbor molecules (n_2–n_5) were from −72.9 to −32.9 kJ mol^{-1} and from −82.9 to −28.7 kJ mol^{-1} in **1** and **2**, respectively. In these π-stacking interactions, the main stabilization term arises from electrostatic and dispersion energies, whereas the destabilization one comes from exchange-repulsion energy. Although the dispersion energies decrease in the order of the distances between the molecules, the electrostatic energies are widely varied from almost zero to −97.0 and −52.9 kJ mol^{-1} for **1** and **2**, respectively. As compared among the π-stacking interactions, the stronger stabilization in electrostatic energy is observed in the π-overlaps concerning the quinolyl ring in the qnal and qsal ligands, whereas the electrostatic stabilization is relatively weak in the π-overlaps between the phenyl rings in the azp ligand. Therefore, the π-stacking interactions involved in the quinolyl ring are much stronger. This may account for given similar π-stacking structures in the homoleptic Fe(qnal)$_2$ and Fe(qsal)$_2$ complexes.[33,34]

The interaction energies between the next-nearest neighbor molecules (nn_1–nn_5) for **1** and **2** are also listed in Table 2. Note that the intermolecular interaction energies E_{tot} stronger than −10 kJ mol^{-1} were found out between the next-nearest neighbor molecules in **1** and **2**. The largest total interaction energies between the next-nearest neighbor molecules are a half or one third less than the smallest interaction energies between the nearest neighbor molecules. As seen in the details of the next-nearest neighbor interactions, a significant decrease in exchange-repulsion energy due to no direct short contact between the molecules and a moderate stabilization by dispersion energy lead to the existence of meaningful interaction energies between the next-nearest neighbor molecules. Recently the importance of dispersion interaction to attractive intermolecular interactions between extended π-conjugated molecules was pointed out by Tsuzuki et al.[35] In particular, the relationship between the nearest and next-nearest neighbor interactions in the literature is consistent with the present results.

The lattice energy H_{lat} of a crystal is the summation of the interaction energies between all the molecules in the whole crystal. Thus, H_{lat} is calculated by the sum of interaction energies E_{tot} of one molecule to all the other molecules expressed by

$$H_{lat} = \sum \frac{E_{tot} \times N}{f} = \sum E_{lat} \cdots (3)$$

where N is the number of the molecule of the same environment, f is the multiple count factor of the same interaction, namely $f = 2$ for the interactions between the Fe(III) complex molecules and $f = 4$ for those between the Fe(III) complex molecule and one of the disordered methanol molecules. Thus, the contribution of each intermolecular interaction energy to the total lattice energy is the expression in the summation, which is designated as E_{lat} in equation (3) and are listed in Tables 2 and S5–S7. Accordingly, the lattice energies H_{lat} were calculated by the summation of E_{lat} in the ascending order of the separation of molecular centroid R until H_{lat} is converged. The lattice energies for the LS and HS states in **1** are −260.7 and −243.7 kJ mol^{-1}, respectively. Meanwhile, the lattice energies for the LS and HS states in **2** are −233.6 and −223.3 kJ mol^{-1}, respectively. Thus, the lattice energy differences $\Delta_{lat}H$ are 17.0 and 10.3 kJ mol^{-1} for **1** and **2**, respectively.

DISCUSSION

All the thermodynamic parameters obtained are summarized in Table 3. To interpret the SCO transitions in **1** and **2** from the thermodynamic point of view, the SCO transition enthalpy $\Delta_{cry}H$ and entropy $\Delta_{cry}S$ are decomposed as follows:

$$\begin{aligned} \Delta_{cry}H &= \Delta_{mol}H + \Delta_{lat}H \\ \Delta_{cry}S &= \Delta_{mol}S + \Delta_{lat}S \end{aligned} \cdots (4)$$

where $\Delta_{mol}H$ and $\Delta_{mol}S$ are the molecular terms and $\Delta_{lat}H$ and $\Delta_{lat}S$ are the crystal-lattice terms. In addition, the SCO transition enthalpy $\Delta_{solu}H$ and entropy $\Delta_{solu}S$ in the solution-state can be decomposed as follows:

$$\begin{aligned} \Delta_{solu}H &= \Delta_{mol}H + \Delta_{solvent}H \\ \Delta_{solu}S &= \Delta_{mol}S + \Delta_{solvent}S \end{aligned} \cdots (5)$$

where $\Delta_{solvent}H$ and $\Delta_{solvent}S$ are the solvent effects on $\Delta_{mol}H$ and $\Delta_{mol}S$. The literature stated that the solvent effect on SCO transition in a diluted solution is modest[36] or the use of different non-interacting solvents should cause only small perturbation.[37] Since we compare $\Delta_{solu}H$ between the similar derivatives **1** and **2** in the same solvent, we assumed that the solvent effects $\Delta_{solvent}H$ on **1** and **2** may be regarded as a constant value. On the other hand, the entropy terms in the solution-state are smaller values and thus are strongly deviated by solvation. Thus, we herein discuss the SCO phenomena using the SCO transition enthalpy and entropy in the solid-state and the SCO transition enthalpy in the solution-state.

Table 3. Thermodynamic Parameters for **1** and **2**

Compounds	**1**	**2**
$\Delta_{cry}H$ / kJ mol^{-1}	9.29	5.33[a]
$\Delta_{cry}S$ / J K^{-1} mol^{-1}	31.2	28.7[a]
Γ_{cry} / kJ mol^{-1}	5.02	3.50[a]
$\Delta_{solu}H$ / kJ mol^{-1}	8.20	11.8
$\Delta_{solu}S$ / J K^{-1} mol^{-1}	35.5	55.6
$\Delta_{lat}H$ / kJ mol^{-1}	17.0	10.3

[a] reference 28.

When the enthalpy difference $\Delta_{cry}H$ in the solid-state was compared with the enthalpy difference $\Delta_{solu}H$ in the solution-state, $\Delta_{cry}H$ was similar to $\Delta_{solu}H$ for **1**, whereas $\Delta_{cry}H$ was one-half as large as $\Delta_{solu}H$ for **2**. This disagreement suggests that only $\Delta_{mol}H$ may not govern $\Delta_{cry}H$. The sums of $\Delta_{solul}H$ and $\Delta_{lat}H$ for **1** and **2** were not equal to the corresponding enthalpy differences $\Delta_{cry}H$. The deviations may arise from the accuracy to estimate $\Delta_{lat}H$ and the solvent effect $\Delta_{solvent}H$. On the other hand, the descending degree of magnitude of $\Delta_{cry}H$ between **1** and **2** resembles that of the sum of $\Delta_{solu}H$ and $\Delta_{lat}H$. It should be noted that the difference in the sum of $\Delta_{solu}H$ and $\Delta_{lat}H$ between **1** and **2** is 3.10 kJ mol^{-1}, which is in an excellent agreement with the difference in $\Delta_{cry}H$ of 3.96 kJ mol^{-1} between **1** and **2**. This suggests that $\Delta_{solu}H$ has a linear relationship to $\Delta_{mol}H$ in the similar molecules in the same solvent and thus $\Delta_{solu}H$ reflects the molecular term. Consequently, the lattice enthalpy difference would play a crucial role in the enthalpy difference in the SCO transition.

The contribution of intermolecular interaction energies to the lattice enthalpy difference $\Delta_{lat}H$ can clarify the role of intermolecular interactions for the SCO transition. The contributions of interaction energies E_{lat} to the lattice enthalpy H_{lat} for **1** and **2** are depicted as bar graphs in Figures 6a and 6b, respectively. As is expected, one can recognize a large contribution of the nearest neighbor interactions to the total lattice enthalpy for both complexes. Next, we should focus on the contributions to the lattice enthalpy difference $\Delta_{lat}H$ in the SCO transition. To decompose the lattice enthalpy difference $\Delta_{lat}H$, we focused on the interaction energy difference $\Delta_{lat}E$:

$$\Delta_{lat}E = E_{lat}(\mathrm{HS}) - E_{lat}(\mathrm{LS}) \cdots (6)$$

where E_{lat}(LS) and E_{lat}(HS) are the interaction energies in the LS and HS states at the same positions, respectively (Table 2). A positive value of $\Delta_{lat}E$ stabilizes the low-temperature structure and/or destabilizes the high-temperature structures, whereas a negative value of $\Delta_{lat}E$ diminishes $\Delta_{lat}H$. For **1** the sum of the nearest neighbor interactions of n_1–n_5 is positive and is about 55% of the total lattice enthalpy difference $\Delta_{lat}H$ of 17.0 kJmol^{-1}, whereas the sum of the next-nearest neighbor interactions of nn_1 and nn_2 is also positive and is 35% of $\Delta_{lat}H$. Thus, the next-nearest neighbor interactions as well as the nearest neighbor interactions may account for the lattice enthalpy difference $\Delta_{lat}H$ on the SCO transition.

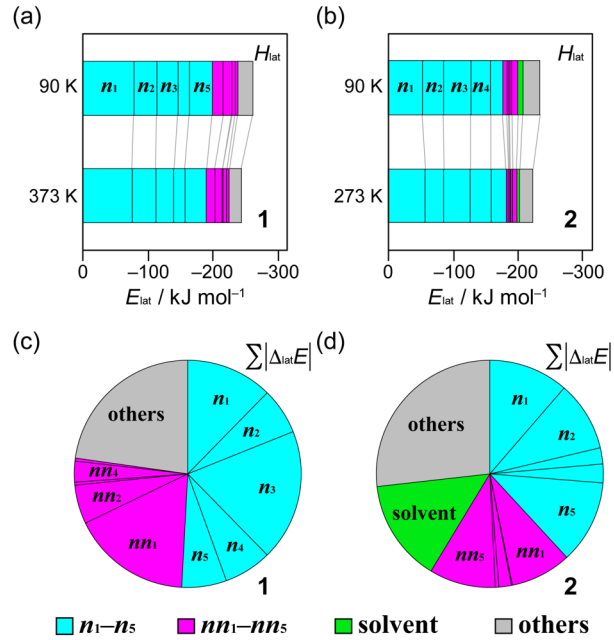

Figure 6. Contributions of intermolecular interaction energies to the total lattice enthalpy for **1** (a) and **2** (b). Proportions of absolute intermolecular interaction energy differences to the total of absolute intermolecular interaction energy differences for **1** (c) and **2** (d). The nearest neighbor and the next-nearest neighbor interaction energy contributions indicate cyan and magenta, respectively. The interaction energy contributions between the Fe(III) complex and methanol molecules in **2** indicate green.

On the other hand, the sum of $\Delta_{lat}E$ is not a good indicator for the contribution of intermolecular interactions to $\Delta_{lat}H$, because the intermolecular interaction energy differences $\Delta_{lat}E$ are varied from positive to negative values. If the intermolecular interaction energy differences $\Delta_{lat}E$ contain both positive and negative values, a positive value of $\Delta_{lat}H$ may be canceled by negative values of $\Delta_{lat}E$. To clarify which intermolecular interaction energies are changed before and after the SCO transition, we can visualize the circle graph using the proportion of each absolute value of $\Delta_{lat}E$ to the total of absolute values of $\Delta_{lat}E$. The circle graph for **1** is shown in Figure 6c. Note that the proportion of the nearest neighbor interactions is one half of the total absolute difference, whereas that of the next-nearest neighbor interactions occupies one-fourth of the total absolute difference. This observation is consistent with the bar graph shown in Figure 6a because only one small negative value of $\Delta_{lat}E$ is found in **1**. Therefore, a relatively large contribution of the next-nearest neighbor interactions to $\Delta_{lat}H$ is evident.

The difference between the above mentioned two ideas is particularly noticeable in the case of the solvate compound **2**. Although the total lattice enthalpy difference $\Delta_{lat}H$ in **2** was positive, the sum of $\Delta_{lat}E$ of the nearest neighbor interactions is negative, indicating that the nearest neighbor interactions relatively stabilize the high-temperature structure probably due to the existence of the solvate molecules. On the other hand, the sum of $\Delta_{lat}E$ of the next-nearest neighbor interactions (nn_1 and nn_5) are meaningfully positive, resulting in a positive value of $\Delta_{lat}H$. Thus, the compensation of $\Delta_{lat}E$ took place in **2**. The proportion of each absolute value of $\Delta_{lat}E$ to the total of absolute values of $\Delta_{lat}E$ in **2** is shown in Figure 6d. We can see the large proportions of both the next-nearest neighbor interac-

tions and the interactions with the solvate molecules to the total of absolute interaction energy differences $\Delta_{lat}E$. The proportion of the next-nearest neighbor interactions and the interactions with the solvate molecules is comparable to that of the nearest neighbor interactions. These observations in **1** and **2** reveal that the change in the next-nearest neighbor interactions would make a significant impact on the lattice enthalpy difference $\Delta_{lat}H$ in the SCO transition. As mentioned in the computational analysis, the stabilization of the next-nearest neighbor interactions originates mainly from dispersion energy. Therefore, the next-nearest neighbor dispersion interactions would play an important role in the enthalpy difference $\Delta_{cry}H$ in the SCO transition.

Finally, we should comment on an SCO transition temperature. The SCO transition temperature T_{SCO} is given by enthalpy difference $\Delta_{cry}H$ divided by entropy difference $\Delta_{cry}S$. Theoretical entropy difference from spin multiplicity in Fe(III) SCO complexes is 9.13 J K^{-1} mol^{-1} and thus large vibrational contributions to the entropy differences $\Delta_{cry}S$ in **1** and **2** are manifested. Since the entropy differences $\Delta_{cry}S$ in **1** and **2** are similar to each other, the transition temperatures would be governed by the enthalpy differences $\Delta_{cry}H$. The computational analysis of intermolecular interactions in **1** and **2** revealed that the π-extension of the ligand results in the enhancement of the intermolecular interaction between the π-extended ligands. However, the conclusion that the π-extension effect may increase the transition temperature is a mistake because the transition temperature and interaction energy are related to $\Delta_{cry}H$ and E_{tot}, respectively. According to the discussion mentioned above, $\Delta_{cry}H$ must include the contribution of both $\Delta_{mol}H$ and $\Delta_{lat}H$. This means that $\Delta_{cry}H$ originates from the total of the change in the molecular electronic state and all intermolecular interactions. Therefore, the isostructural or isomorphous compounds must be compared to clarify the genuine substituted effect of π-extension in the solid-state. In the present case, complex **1** was the solvate compound, whereas complex **2** was the non-solvate one. Therefore, we cannot compare the transition temperatures between **1** and **2** directly. The increase in the transition temperature in **1** should be interpreted to result from the total of the change in all the intermolecular interactions induced by the π-extension and solvate effects.

CONCLUSION

We report here the synthesis, structural and physical characterizations of a novel neutral π-extended heteroleptic Fe(III) compound **1** exhibiting a cooperative SCO transition exactly at room temperature. The experimental thermodynamic analysis of compound **1** along with the parent compound **2** revealed that the enthalpy difference in the SCO transition can be composed of the enthalpy differences from the single-molecule and crystal-lattice. The computational analysis of intermolecular interactions discloses that the next-nearest neighbor interactions as well as the conventional nearest neighbor π-stacking interactions play a significant role in the lattice enthalpy difference in the SCO transition. So far the intermolecular interactions judging from shorter atom-atom distances than the sum of their van der Waals radii have been taken into account to govern the crystal structure and property of a molecular solid. Therefore, the present findings shed light on the possibility of the crucial role of the next-nearest neighbor dispersion interactions upon the SCO transition. We should notice that a more accurate quantum mechanical calculation must be required to estimate accurate intermolecular interaction energies. This finding may be extended to the cases that most molecular solids including ionic compounds undergo a phase transition. We are convinced that the computational evaluation of intermolecular interactions can open the door to unfold the fundamental mechanism of a solid-state phase transition in molecular materials.

ASSOCIATED CONTENT

Supporting Information

The Supporting Information is available free of charge on the ACS Publications website.

Synthesis, physical measurement details, and computational calculation methods, including Figures S1–S3 and Tables S1–S7 (PDF)
Crystal Structures for **1** at 90 and 373 K (CIF)

AUTHOR INFORMATION

Corresponding Author

* ktaka@crystal.kobe-u.ac.jp

ACKNOWLEDGMENT

K. T. is grateful to Prof. Yoshihito Shiota at Kyushu University for discussion about the theoretical calculations. This work was partially supported by a Grant-in-Aid for Scientific Research (C) (No. 19K05402) from the Ministry of Education, Culture, Sports, Science, and Technology of Japan, and a grant from CASIO foundation. This work was carried out by the joint research program of Molecular Photoscience Research Center, Kobe University.

REFERENCES

(1) *Spin Crossover in Transition Metal Compounds I−III*; Gütlich, P.; Goodwin, H. A., Eds.; Topics in Current Chemistry; Springer: Berlin/Heidelberg, Germany, 2004.

(2) *Spin-Crossover Materials*; Halcrow, M. A., Ed.; John Wiley & Sons, Ltd.: Oxford, UK, 2013.

(3) Gütlich, P.; Gaspar, A. B.; Garcia, Y. Spin State Switching in Iron Coordination Compounds. *Beilstein J. Org. Chem.* **2013**, *9* (II), 342–391.

(4) Manrique-Juarez, M. D.; Mathieu, F.; Shalabaeva, V.; Cacheux, J.; Rat, S.; Nicu, L.; Leïchlé, T.; Salmon, L.; Molnár, G.; Bousseksou, A. A Bistable Microelectromechanical System Actuated by Spin-Crossover Molecules. *Angew. Chemie Int. Ed.* **2017**, *56* (28), 8074–8078.

(5) Mikolasek, M.; Manrique-Juarez, M. D.; Shepherd, H. J.; Ridier, K.; Rat, S.; Shalabaeva, V.; Bas, A.-C.; Collings, I. E.; Mathieu, F.; Cacheux, J.; et al. Complete Set of Elastic Moduli of a Spin-Crossover Solid: Spin-State Dependence and Mechanical Actuation. *J. Am. Chem. Soc.* **2018**, *140* (28), 8970–8979.

(6) Takahashi, K.; Cui, H.-B.; Okano, Y.; Kobayashi, H.; Einaga, Y.; Sato, O. Electrical Conductivity Modulation Coupled to a High-Spin−Low-Spin Conversion in the Molecular System $[Fe^{III}(qsal)_2][Ni(dmit)_2]_3 \cdot CH_3CN \cdot H_2O$. *Inorg. Chem.* **2006**, *45* (15), 5739–5741.

(7) Takahashi, K.; Cui, H.-B.; Okano, Y.; Kobayashi, H.; Mori, H.; Tajima, H.; Einaga, Y.; Sato, O. Evidence of the Chemical Uniaxial Strain Effect on Electrical Conductivity in the Spin-Crossover Conducting Molecular System: $[Fe^{III}(qnal)_2][Pd(dmit)_2]_5 \cdot$Acetone. *J. Am. Chem. Soc.* **2008**, *130* (21), 6688–6689.

(8) Phan, H.; Benjamin, S. M.; Steven, E.; Brooks, J. S.; Shatruk, M. Photomagnetic Response in Highly Conductive Iron(II) Spin-Crossover Complexes with TCNQ Radicals. *Angew. Chem. Int. Ed.* **2015**, *54* (3), 823–827.

(9) Nihei, M.; Tahira, H.; Takahashi, N.; Otake, Y.; Yamamura, Y.; Saito, K.; Oshio, H. Multiple Bistability and Tristability with Dual

Spin-State Conversions in $[Fe(dpp)_2][Ni(mnt)_2]_2 \cdot MeNO_2$. *J. Am. Chem. Soc.* **2010**, *132* (10), 3553–3560.

(10) Ohkoshi, S.; Imoto, K.; Tsunobuchi, Y.; Takano, S.; Tokoro, H. Light-Induced Spin-Crossover Magnet. *Nat. Chem.* **2011**, *3* (7), 564–569.

(11) Ababei, R.; Pichon, C.; Roubeau, O.; Li, Y.-G.; Bréfuel, N.; Buisson, L.; Guionneau, P.; Mathonière, C.; Clérac, R. Rational Design of a Photomagnetic Chain: Bridging Single-Molecule Magnets with a Spin-Crossover Complex. *J. Am. Chem. Soc.* **2013**, *135* (39), 14840–14853.

(12) Fukuroi, K.; Takahashi, K.; Mochida, T.; Sakurai, T.; Ohta, H.; Yamamoto, T.; Einaga, Y.; Mori, H. Synergistic Spin Transition between Spin Crossover and Spin-Peierls-like Singlet Formation in the Halogen-Bonded Molecular Hybrid System: $[Fe(Iqsal)_2][Ni(dmit)_2] \cdot CH_3CN \cdot H_2O$. *Angew. Chem. Int. Ed.* **2014**, *53* (7), 1983–1986.

(13) Jornet-Mollá, V.; Duan, Y.; Giménez-Saiz, C.; Tang, Y.-Y. Y.; Li, P.-F. F.; Romero, F. M.; Xiong, R.-G. G. A Ferroelectric Iron(II) Spin Crossover Material. *Angew. Chem. Int. Ed.* **2017**, *56* (45), 14052–14056.

(14) Ohkoshi, S. I.; Takano, S.; Imoto, K.; Yoshikiyo, M.; Namai, A.; Tokoro, H. 90-Degree Optical Switching of Output Second-Harmonic Light in Chiral Photomagnet. *Nat. Photonics* **2014**, *8* (1), 65–71.

(15) Lochenie, C.; Schötz, K.; Panzer, F.; Kurz, H.; Maier, B.; Puchtler, F.; Agarwal, S.; Köhler, A.; Weber, B. Spin-Crossover Iron(II) Coordination Polymer with Fluorescent Properties: Correlation between Emission Properties and Spin State. *J. Am. Chem. Soc.* **2018**, *140* (2), 700–709.

(16) Wang, C.-F.; Yang, G.-Y.; Yao, Z.-S.; Tao, J. Monitoring the Spin States of Ferrous Ions by Fluorescence Spectroscopy in Spin-Crossover-Fluorescent Hybrid Materials. *Chem. - A Eur. J.* **2018**, *24* (13), 3218–3224.

(17) Iasco, O.; Rivière, E.; Guillot, R.; Buron-Le Cointe, M.; Meunier, J.-F.; Bousseksou, A.; Boillot, M.-L. $Fe^{II}(pap\text{-}5NO_2)_2$ and $Fe^{II}(qsal\text{-}5NO_2)_2$ Schiff-Base Spin-Crossover Complexes: A Rare Example with Photomagnetism and Room-Temperature Bistability. *Inorg. Chem.* **2015**, *54* (4), 1791–1799.

(18) Phonsri, W.; Davies, C. G.; Jameson, G. N. L.; Moubaraki, B.; Ward, J. S.; Kruger, P. E.; Chastanet, G.; Murray, K. S. Symmetry Breaking above Room Temperature in an Fe(II) Spin Crossover Complex with an N_4O_2 Donor Set. *Chem. Commun.* **2017**, *53* (8), 1374–1377.

(19) Bousseksou, A.; McGarvey, J. J.; Varret, F.; Real, J. A.; Tuchagues, J.; Dennis, A. C.; Boillot, M. L. Raman Spectroscopy of the High- and Low-Spin States of the Spin Crossover Complex $Fe(phen)_2(NCS)_2$: An Initial Approach to Estimation of Vibrational Contributions to the Associated Entropy Change. *Chem. Phys. Lett.* **2000**, *318* (4–5), 409–416.

(20) Brehm, G.; Reiher, M.; Schneider, S. Estimation of the Vibrational Contribution to the Entropy Change Associated with the Low- to High-Spin Transition in $Fe(phen)_2(NCS)_2$ Complexes: Results Obtained by IR and Raman Spectroscopy and DFT Calculations. *J. Phys. Chem. A* **2002**, *106* (50), 12024–12034.

(21) Gütlich, P.; Hauser, A.; Spiering, H. Thermal and Optical Switching of Iron(II) Complexes. *Angew. Chem. Int. Ed.* **1994**, *33* (20), 2024–2054.

(22) Takahashi, K.; Okai, M.; Mochida, T.; Sakurai, T.; Ohta, H.; Yamamoto, T.; Einaga, Y.; Shiota, Y.; Yoshizawa, K.; Konaka, H.; et al. Contribution of Coulomb Interactions to a Two-Step Crystal Structure Phase Transformation Coupled with a Significant Change in Spin Crossover Behavior for a Series of Charged Fe^{II} Complexes from 2,6-Bis(2-methylthiazol-4-yl)pyridine. *Inorg. Chem.* **2018**, *57* (3), 1277–1287.

(23) Vela, S.; Paulsen, H. Deciphering Crystal Packing Effects in the Spin Crossover of Six $[Fe^{II}(2\text{-}Pic)_3]Cl_2$ Solvatomorphs. *Dalton Trans.* **2019**, *48* (4), 1237–1245.

(24) Turner, M. J.; McKinnon, J. J.; Wolff, S. K.; Grimwood, D. J.; Spackman, P. R.; Jayatilaka, D.; Spackman, M. A. CrystalExplorer17 (2017). University of Western Australia. http://hirshfeldsurface.net.

(25) Turner, M. J.; Grabowsky, S.; Jayatilaka, D.; Spackman, M. A. Accurate and Efficient Model Energies for Exploring Intermolecular Interactions in Molecular Crystals. *J. Phys. Chem. Lett.* **2014**, *5* (24), 4249–4255.

(26) Mackenzie, C. F.; Spackman, P. R.; Jayatilaka, D.; Spackman, M. A. CrystalExplorer Model Energies and Energy Frameworks: Extension to Metal Coordination Compounds, Organic Salts, Solvates and Open-Shell Systems. *IUCrJ* **2017**, *4* (5), 575–587.

(27) Thomas, S. P.; Spackman, P. R.; Jayatilaka, D.; Spackman, M. A. Accurate Lattice Energies for Molecular Crystals from Experimental Crystal Structures. *J. Chem. Theory Comput.* **2018**, *14* (3), 1614–1623.

(28) Murata, S.; Takahashi, K.; Mochida, T.; Sakurai, T.; Ohta, H.; Yamamoto, T.; Einaga, Y. Cooperative Spin-Crossover Transition from Three-Dimensional Purely π-Stacking Interactions in a Neutral Heteroleptic Azobisphenolate Fe^{III} Complex with a N_3O_3 Coordination Sphere. *Dalton Trans.* **2017**, *46* (18), 5786–5789.

(29) Takahashi, K.; Kawamukai, K.; Okai, M.; Mochida, T.; Sakurai, T.; Ohta, H.; Yamamoto, T.; Einaga, Y.; Shiota, Y.; Yoshizawa, K. A New Family of Anionic Fe^{III} Spin Crossover Complexes Featuring a Weak-Field N_2O_4 Coordination Octahedron. *Chem. Eur. J.* **2016**, *22* (4), 1253–1257.

(30) Takahashi, K.; Yamamoto, K.; Yamamoto, T.; Einaga, Y.; Shiota, Y.; Yoshizawa, K.; Mori, H. High-Temperature Cooperative Spin Crossover Transitions and Single-Crystal Reflection Spectra of $[Fe^{III}(qsal)_2](CH_3OSO_3)$ and Related Compounds. *Crystals* **2019**, *9* (2), 81.

(31) Schubert, E. M. Utilizing the Evans Method with a Superconducting NMR Spectrometer in the Undergraduate Laboratory. *J. Chem. Educ.* **1992**, *69* (1), 62.

(32) Slichter, C. P.; Drickamer, H. G. Pressure-Induced Electronic Changes in Compounds of Iron. *J. Chem. Phys.* **1972**, *56* (5), 2142–2160.

(33) Tsukiashi, A.; Nakaya, M.; Kobayashi, F.; Ohtani, R.; Nakamura, M.; Harrowfield, J. M.; Kim, Y.; Hayami, S. Intermolecular Interaction Tuning of Spin-Crossover Iron(III) Complexes with Aromatic Counteranions. *Inorg. Chem.* **2018**, *57* (5), 2834–2842.

(34) Takahashi, K.; Yamamoto, K.; Yamamoto, T.; Einaga, Y.; Shiota, Y.; Yoshizawa, K.; Mori, H. High-Temperature Cooperative Spin Crossover Transitions and Single-Crystal Reflection Spectra of $[Fe^{III}(qsal)_2](CH_3OSO_3)$ and Related Compounds. *Crystals* **2019**, *9* (2), 81.

(35) Tsuzuki, S.; Orita, H.; Sato, N. Intermolecular Interactions of Oligothienoacenes: Do S···S Interactions Positively Contribute to Crystal Structures of Sulfur-Containing Aromatic Molecules? *J. Chem. Phys.* **2016**, *145* (17), 174503.

(36) Toftlund, H. Spin Equilibrium in Solutions. *Monatsh. Chem.* **2001**, *132* (11), 1269–1277s.

(37) Kershaw Cook, L. J.; Kulmaczewski, R.; Mohammed, R.; Dudley, S.; Barrett, S. A.; Little, M. A.; Deeth, R. J.; Halcrow, M. A. A Unified Treatment of the Relationship Between Ligand Substituents and Spin State in a Family of Iron(II) Complexes. *Angew. Chem. Int. Ed.* **2016**, *55* (13), 4327–4331.

For Table of Contents Only
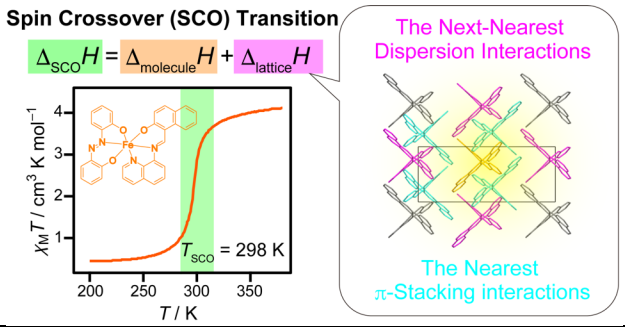
A new π-extended heteroleptic complex from the azobisphenolate ligand exhibited an abrupt spin-crossover transition exactly at room temperature. The comparison of experimental and computational analyses with the parent compound revealed that the next-nearest neighbor dispersion interactions as well as the conventional nearest neighbor π-stacking interactions may play an significant role in the solid-state SCO transition enthalpy.